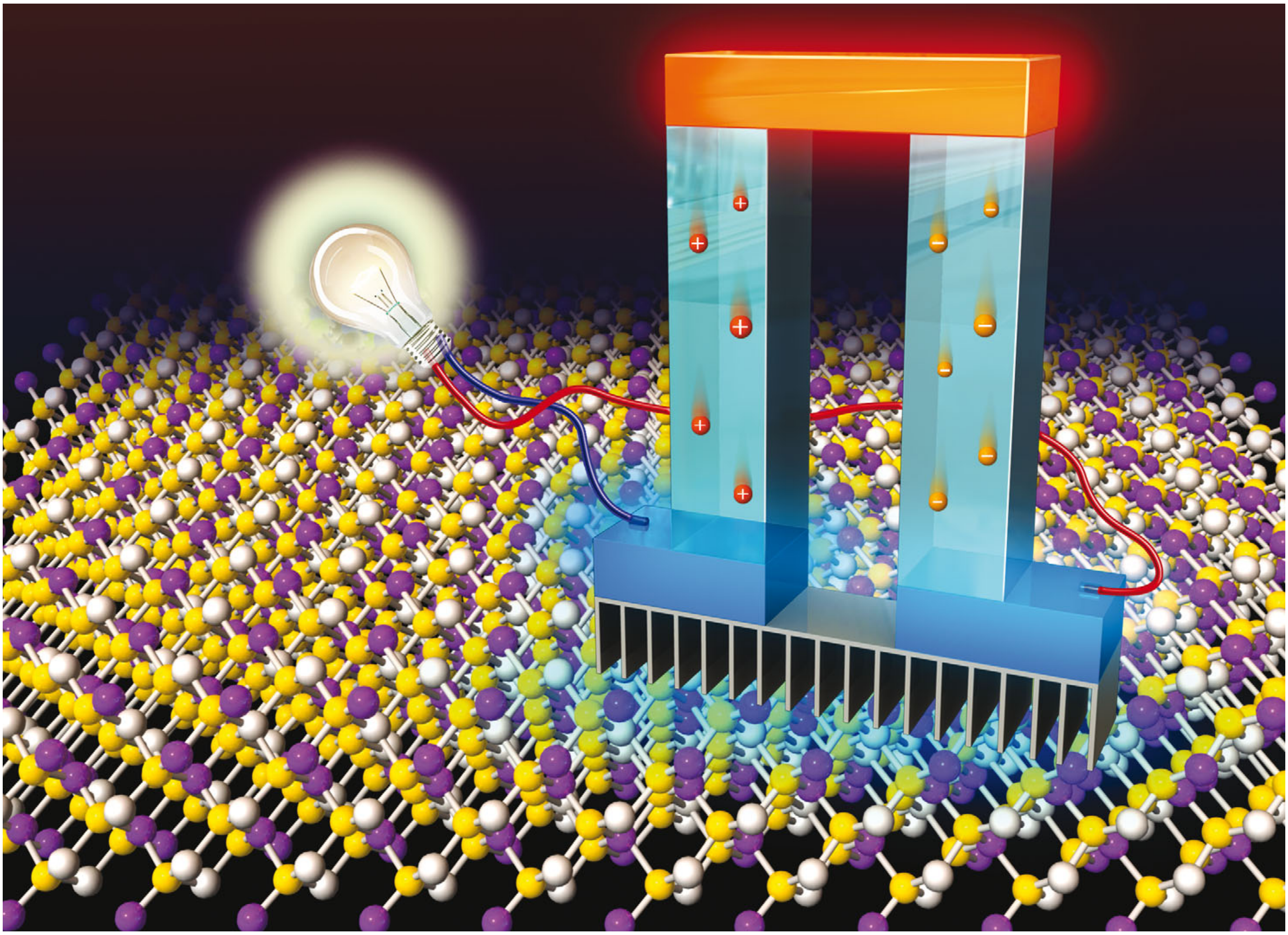

Showcasing research from Prof. Dong Wang's group at the Department of Chemistry, Tsinghua University, Beijing, P. R. China.

Title: High thermoelectric performance from optimization of hole-doped CuInTe$_2$

The electronic structure, lattice dynamics and thermoelectric transport properties of a ternary compound CuInTe$_2$ have been investigated from first-principles. Either p-doping at the In-site or n-doping at the Cu-site barely modifies the electronic states near the valence or conduction band edge but increases the carrier concentration to achieve the highest thermoelectric efficiency. The thermal conductivity of CuInTe$_2$ can be effectively reduced by introducing structural defects at Cu, In and Te sites. By doping optimization, p-type CuInTe$_2$ are promising thermoelectric materials for waste heat recovery at medium temperatures.

As featured in:

See Gang Zhou and Dong Wang, *Phys. Chem. Chem. Phys.*, 2016, **18**, 5925.

ROYAL SOCIETY
OF **CHEMISTRY**

www.rsc.org/pccp

Registered charity number: 207890

Published on 09 November 2015. Downloaded by Tsinghua University on 21/05/2018 02:33:05.

PCCP

PAPER

View Article Online
View Journal | View Issue

Cite this: *Phys. Chem. Chem. Phys.*, 2016, **18**, 5925

Received 28th August 2015, Accepted 9th November 2015

DOI: 10.1039/c5cp05129k

www.rsc.org/pccp

High thermoelectric performance from optimization of hole-doped $CuInTe_2$

Gang Zhou and Dong Wang*

We investigated the electronic structure, lattice dynamics and thermoelectric transport properties of $CuInTe_2$ based on first-principles calculations. From the analysis of density of states and partial charge density, it can be expected that p-doping at the In-site or n-doping at the Cu-site will barely modify the electronic states near the valence or conduction band edge but increase the carrier concentration to achieve the highest thermoelectric efficiency. Lattice dynamics calculations suggest that the thermal conductivity of $CuInTe_2$ can be effectively reduced by introducing structural defects at Cu, In and Te sites. p-type $CuInTe_2$ possesses better thermoelectric properties as compared to the n-type one, which mainly originates from the steeper density of states resulting from nearly degenerate valence bands near the band edge. The temperature dependence of the thermoelectric transport properties of p-type $CuInTe_2$ at different carrier concentrations was studied in detail, which is found to be in good agreement with the experimental data. Our results of calculation showed that p-type $CuInTe_2$ can achieve an upper-limit figure of merit value of 1.72 at 850 K and are promising thermoelectric materials for waste heat recovery at medium temperatures.

I. Introduction

Under the topic the challenges of global energy crisis and climate change, thermoelectric materials, which can be utilized to directly convert heat into electricity in the solid state, have gained renewed interest in recent years.[1–5] The energy conversion efficiencies of thermoelectric devices are characterized by the dimensionless thermoelectric figure of merit of materials:[1,6] $ZT = S^2\sigma T/\kappa$, where S, σ, T and κ denote the Seebeck coefficient, electrical conductivity, temperature and thermal conductivity, respectively. Both electrons and phonons are heat carriers, therefore the thermal conductivity can be divided into two independent contributions. As a result, there exist two major strategies to improve the thermoelectric efficiency: band structure engineering to optimize the electrical properties[4,6,7] and phonon engineering to decrease the phonon thermal conductivity.[1,7,8] However, the interdependence of Seebeck coefficient, electrical conductivity and electronic thermal conductivity has made the maximization of ZT a challenge so far.[2,3,9]

Recently, a ternary compound $CuInTe_2$ with pseudocubic structures has been reported to exhibit promising thermoelectric properties in the moderate temperature range.[10–12] It was experimentally found that the ZT value of $CuInTe_2$ can reach 1.18 at 850 K.[11] Yang *et al.* have reported that the ZT value of $CuInTe_2$ can be effectively improved by simultaneous substitution of Zn for both Cu and In, and they achieved a ZT value of 0.69 at 737 K, which is 1.65 times that of Zn-free $CuInTe_2$.[13] Chen *et al.* have investigated the thermoelectric properties of $CuInTe_2$/graphene composites and obtained an improved ZT value due to the decreased thermal conductivity.[12] Impurity doping is an effective method to optimize the carrier concentration and improve the thermoelectric properties of materials.[14] First-principles electronic structure calculations can help us to identify the appropriate doping sites to optimize the carrier concentration whereas they do not modify the electronic states of pristine materials. In this work, we have investigated the thermoelectric transport properties of $CuInTe_2$ by using first-principles methods and Boltzmann transport equations. We analyzed how the features in the band structure of $CuInTe_2$ affect the electrical transport properties, and identified the optimal doping sites and level to maximize the thermoelectric performance of $CuInTe_2$. Lattice dynamics analysis also helps us to identify the appropriate sites to introduce the structural defects for further reduction of the lattice thermal conductivity. Our investigations established an upper bound of thermoelectric figure of merit for $CuInTe_2$ and demonstrated that an improvement over the previously reported values is possible under optimal conditions.

MOE Key Laboratory of Organic OptoElectronics and Molecular Engineering, Department of Chemistry, Tsinghua University, Beijing, 100084, People's Republic of China. E-mail: dong913@tsinghua.edu.cn; Tel: +86-10-62798081

Published on 09 November 2015. Downloaded by Tsinghua University on 21/05/2018 02:33:05.

II. Computational methods

The energy band calculations have been performed by using the projector augmented wave (PAW) method within the framework of density functional theory as implemented in the Vienna *Ab initio* Simulation Package (VASP).[15–17] The generalized gradient approximation (GGA) in the Perdew–Burke–Ernzerhof (PBE) functional form[18] was applied. The geometry for $\mathrm{CuInTe_2}$ is fully relaxed until the magnitude of the force acting on all atoms is less than 0.01 eV $\mathrm{\AA^{-1}}$ and the total energy converges within 0.001 meV. The cutoff energy was set to 500 eV for the plane-wave expansion and the Monkhorst–Pack **k**-mesh of 7 × 7 × 7 was adopted for the integration of the Brillouin zone. Being strongly localized, the exchange–correlation effects of the Cu 3d electrons are not adequately described within the generalized gradient approximation. This can be to some extent corrected with the DFT+U method, which is a combination of the DFT and Hubbard Hamiltonian for the Coulomb repulsion. Here we chose the PBE+U method to calculate the electronic structure of $\mathrm{CuInTe_2}$. The effective Coulomb repulsion parameter U was set to 4 eV according to the previously reported value of Cu-based ternary semiconductors.[19]

The phonon properties were derived from the lattice dynamics computations using the *ab initio* force constant method as implemented in the PHONOPY code.[20] Supercells were constructed as a 2 × 2 × 2 tetragonal unit cell, corresponding to 8 unit cells in the tetragonal setting containing 128 atoms. Symmetry-inequivalent atomic displacements were generated to obtain forces from VASP and then phonon frequencies can be derived from second-order force constants, which were obtained by the finite-difference of forces.

On the basis of the electronic band structure, the thermoelectric transport properties can be evaluated by using the semi-classical Boltzmann transport equations with the relaxation time approximation, as implemented in the BoltzTraP code.[21] The thermoelectric transport coefficients σ, S and κ_e can be written in a compact form in terms of the $\Lambda^{(\alpha)}$ function[6,22]

$$\sigma = \Lambda^{(0)}, \tag{1}$$

$$S = -\frac{1}{eT}\left(\frac{\Lambda^{(1)}}{\Lambda_{(0)}}\right), \tag{2}$$

$$\kappa_e = \frac{1}{e^2T}\left\{\Lambda^{(2)} - \frac{\left[\Lambda^{(1)}\right]^2}{\Lambda^{(0)}}\right\}, \tag{3}$$

where

$$\Lambda^{(\alpha)} = \int d\varepsilon\left(-\frac{\partial f_0}{\partial \varepsilon}\right)(\varepsilon - E_F)^{\alpha}\sum(\varepsilon), \tag{4}$$

where e is the elementary charge of the carriers, T is the temperature, E_F is the Fermi level, f_0 is the Fermi–Dirac distribution function, and $\sum(\varepsilon)$ is the transport distribution function which can be expressed as

$$\sum(\varepsilon) = \frac{e^2}{N_{\mathbf{k}}\Omega}\sum_{i,\mathbf{k}}\mathbf{v}_{i,\mathbf{k}}\mathbf{v}_{i,\mathbf{k}}\tau_{i,\mathbf{k}}\delta(\varepsilon - \varepsilon_i(\mathbf{k})), \tag{5}$$

where i and $\mathbf{k}$ are the band index and the wave vector, respectively, $\tau_{i,\mathbf{k}}$ is the relaxation time, $N_{\mathbf{k}}$ is the number of sampled **k** points in the Brillouin zone (BZ), Ω is the volume of the unit cell, and $\mathbf{v}_{i,\mathbf{k}}$ is the group velocity of the carriers in band i with wave vector **k**. The velocity $\mathbf{v}_{i,\mathbf{k}}$ can be determined from a **k**-space gradient

$$\mathbf{v}_{i,\mathbf{k}} = \frac{1}{\hbar}\frac{\partial \varepsilon_i(\mathbf{k})}{\partial \mathbf{k}}, \tag{6}$$

which requires the eigenvalues on a dense **k** mesh for an accurate evaluation.

III. Results and discussion

$\mathrm{CuInTe_2}$ is crystallized in a tetragonal structure with a space group of $I\bar{4}2d$, which may be derived from the diamond-like cubic zinc-blende material.[12] Fig. 1 shows the *ab initio* electronic band structure of $\mathrm{CuInTe_2}$. Our results of the calculation show that the fundamental gap of $\mathrm{CuInTe_2}$ is direct at the Γ-point in the BZ with a magnitude of 0.177 eV (see Fig. 1). In contrast to the zinc blende lattice, the triply degenerate valence band Γ_{15v} in $\mathrm{CuInTe_2}$ splits into a non-degenerate band Γ_{4v} and a doubly degenerate band Γ_{5v} due to the crystal field effect.[10] The tetragonal distortion parameter η (=$c/2a$) of $\mathrm{CuInTe_2}$ is very close to 1, which causes a small crystal field splitting energy.[10] Therefore, the valence bands at the Γ point are nearly triply degenerate. The non-degenerate band Γ_{4v} is a light-hole band while the doubly degenerate band Γ_{5v} is a heavy-hole band. Such a mixture of heavy and light bands near the valence band maximum (VBM) that are nearly degenerate indicates a promising thermoelectric performance for p-type doping.[23,24] In comparison with previous calculations,[23] our calculated crystal field splitting energy is significantly smaller. The conduction bands exhibit strong dispersion near the band edge and then become relatively flat with increasing energy. The calculated band gap is smaller than the experimentally measured gap,[12] which originates from the fact that standard density functional theory usually underestimates the band gaps of semiconductors. In order to achieve a better agreement between theory and experiment, the band gap of $\mathrm{CuInTe_2}$ was adjusted to match the experimental data by applying the so-called scissor operator in our subsequent calculations

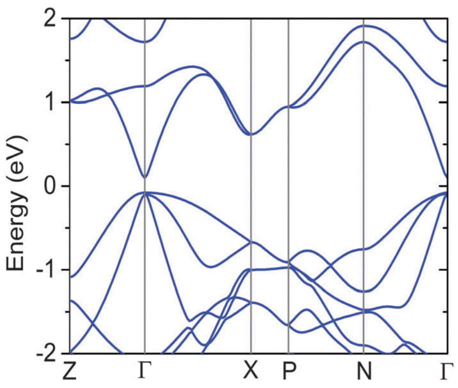

Fig. 1 Band structures of $\mathrm{CuInTe_2}$.

This journal is © the Owner Societies 2016

Published on 09 November 2015. Downloaded by Tsinghua University on 21/05/2018 02:33:05.

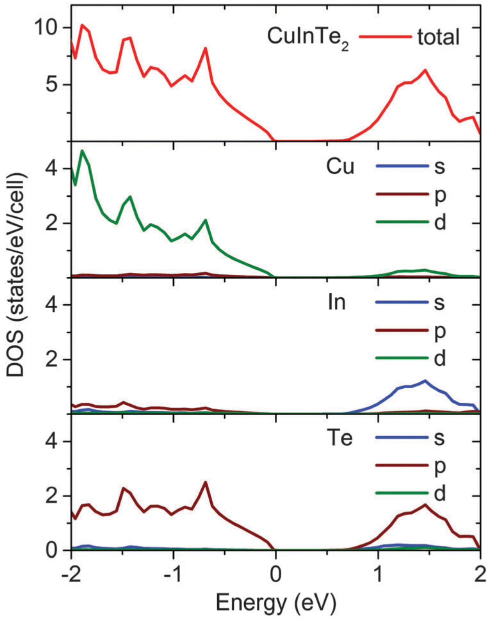

Fig. 2 Total and atom-projected densities of states of CuInTe$_2$.

of transport properties. Similar treatments have been widely adopted in previous calculations.[25,26] The scissor operator does not change the band dispersion and group velocities, so the only influence of band gap adjustment is on the carrier concentration dependence of Seebeck coefficients. When the Fermi level is in the gap and the carrier concentration is low, both conduction and valence bands may contribute to the Seebeck coefficients with opposite signs, resulting in a drop of the Seebeck coefficients at low carrier concentrations. This is known as the bipolar effect. Without the band gap adjustment, the bipolar effect will be more pronounced since the band gap is underestimated.

We plotted the total and atom-projected densities of states (DOSs) of CuInTe$_2$ in Fig. 2. It can be seen from Fig. 2 that the energy states near the valence band edge primarily come from the hybridization of 3d orbitals of Cu atoms and 5p orbitals of Te atoms, which form a conducting pathway for charge carriers in p-type semiconductors. The energy states near the conduction band edge are mainly due to the hybridization of the In 4s and Te 5p orbitals, which can provide a conducting pathway for charge carriers in n-type semiconductors. The total DOS near the valence band edge is steeper while that near the conduction band edge is very flat at first then becomes steep with increasing energy, as in the band structures. It can be expected that a steep slope of DOS near the band gap should lead to a high Seebeck coefficient.[24,26,27]

To further identify the optimal doping sites, the partial charge densities for the bands near the Fermi level are illustrated in Fig. 3. The left panel of Fig. 3 shows that electrons are mostly distributed around the Cu and Te atoms and those around In atoms are nearly invisible, which is in accordance with the atom-projected DOS. Thus, p-doping at the In site will not substantially modify the electronic structures near the edge of valence bands, which provides us a doping site to optimize the carrier concentration to improve the thermoelectric figure of merit of CuInTe$_2$.

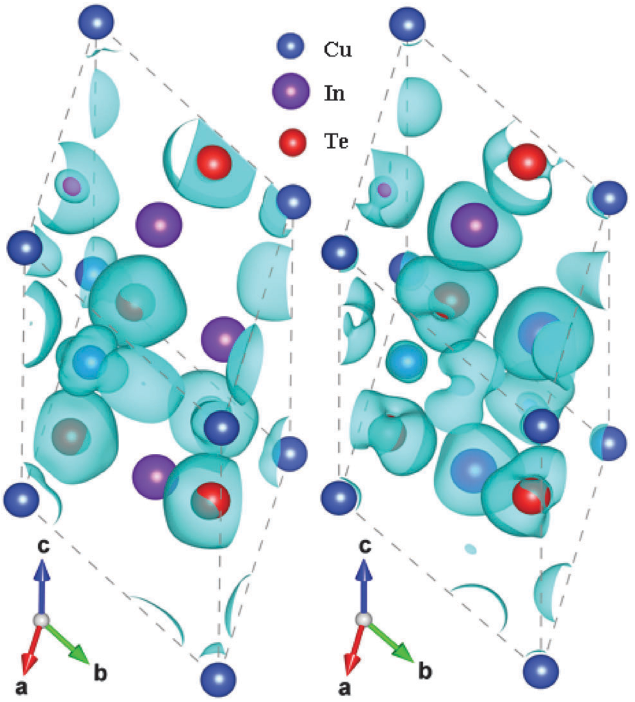

Fig. 3 Partial charge density of CuInTe$_2$ for the bands near the Fermi level. The left panel represents the upper parts of valence bands within a 2 eV window below the VBM, with an isosurface value of 0.0025 e bohr^{-3}; the right panel represents the lower parts of conduction bands within a 2 eV window above the CBM, with an isosurface value of 0.0035 e bohr^{-3}.

The right panel of Fig. 3 shows that the charge density mainly distributes around In and Te atoms, forming a [In–Te–In] conducting network for electron transport. This illustrates that n-doping (or substitution) at the Cu-site will only change the carrier concentrations with little effects on the shape of the conduction band minimum (CBM).

The phonon-dispersion curves and the vibrational density of states for CuInTe$_2$ are shown in Fig. 4. Our calculated phonon frequencies are consistent with the experimental data.[28] For example, the lowest optical phonon frequency (48.7 cm^{-1}) at the Γ-point is very close to the experimental value (48 cm^{-1}).[28] The optical phonon modes exhibit weak dispersion, and these flat optical branches contribute negligibly to heat transport because their group velocities are small.[29] As compared to optical phonon modes, the low-frequency acoustic modes below 50 cm^{-1} are highly dispersive and have larger group velocities. Therefore, these heat-carrying acoustic modes will dominate the thermal transport properties in perfect bulk CuInTe$_2$. Fig. 4(a) shows that some optical modes have very low frequencies at around 50 cm^{-1} and are mixed with the acoustic modes. These low lying optical phonon modes will induce scattering due to their anharmonic coupling to the acoustic phonon modes, which can effectively reduce the thermal conductivity of CuInTe$_2$.[30] It can be seen from Fig. 4(b) that the modes are mixed states composed of Cu, In, and Te atoms in the whole range of frequency and Te atoms have the largest contribution to the total phonon DOS except for a frequency range from 127 cm^{-1} to 147 cm^{-1}. Besides, either Cu, In, or Te

Published on 09 November 2015. Downloaded by Tsinghua University on 21/05/2018 02:33:05.

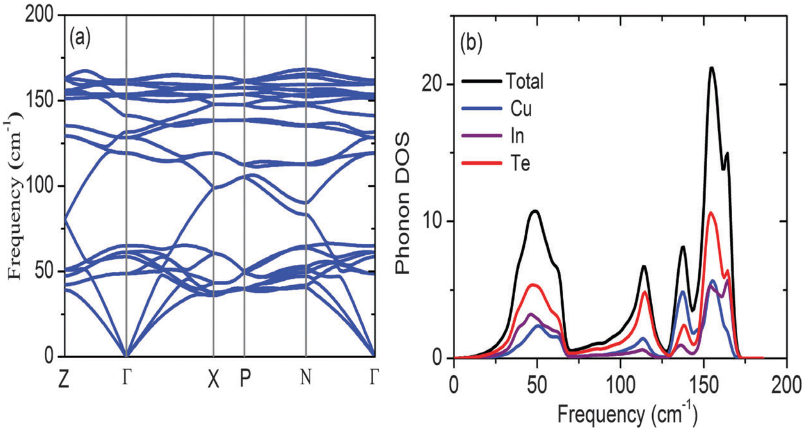

Fig. 4 Phonon dispersion curves (a) and total density of states (b) for CuInTe$_2$. The partial phonon DOS projected onto Cu, In and Te atoms are also shown.

lattice sites can be used as effective sites to introduce the structural defects to induce additional phonon scattering with low-frequency acoustic modes and thus decrease the phonon thermal conductivity of CuInTe$_2$.

We firstly calculated Seebeck coefficients of CuInTe$_2$ in different crystallographic directions as a function of carrier concentrations at three different temperatures of 300, 600 and 800 K, as shown in Fig. 5(a) and (b). For p-type CuInTe$_2$, the presence of nearly degenerate valence bands near the Fermi level is responsible for this high Seebeck coefficient. For the n-type case, Seebeck coefficients first decrease then increase with the carrier concentration, which is due to the conduction-band dispersion near the Fermi level varying from steep to flat. At all temperatures and carrier concentrations, the Seebeck coefficient of p-type CuInTe$_2$ is larger than that of the n-type one, which mainly originates from the fact that DOS near the edge of the valence band is significantly steeper than that near the edge of the conduction band. Additionally, we find that the Seebeck coefficient is isotropic for p-type CuInTe$_2$ and exhibits a little anisotropy for the n-type one at higher carrier concentrations. From Fig. 5(a), it is found that the magnitude of S decreases with increasing n in the range of carrier concentrations. From the

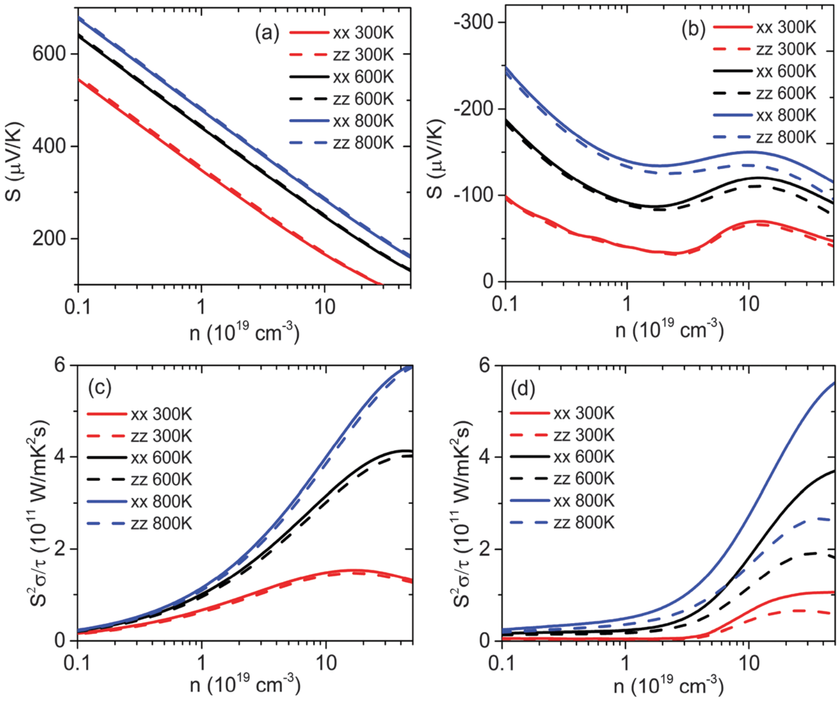

Fig. 5 Anisotropic thermoelectric transport properties of CuInTe$_2$ as a function of carrier concentrations at different temperatures: p-type Seebeck coefficients (a), n-type Seebeck coefficients (b), p-type power factors $S^2\sigma/\tau$ (c), and n-type power factors $S^2\sigma/\tau$ (d). Here the xx and zz directions correspond to the a-axis and the c-axis, respectively.

This journal is © the Owner Societies 2016

Published on 09 November 2015. Downloaded by Tsinghua University on 21/05/2018 02:33:05.

Maxwell–Boltzmann approximation (when $E_F - E_v \gg k_BT$), one can derive an expression for S:[26,31]

$$S = -\frac{k_B}{e}\ln\left(\frac{n}{N_v}\right) + \frac{k_B}{e}A_v \tag{7}$$

where N_v is the effective density of states near the valence band edge and A_v represents a scattering factor. N_v can be expressed as

$$N_v = \int_{-\infty}^{E_v} g_v(\varepsilon)\exp[-(E_v - \varepsilon)/k_BT]\mathrm{d}\varepsilon, \tag{8}$$

where $g_v(\varepsilon)$ is the density of states and E_v is the valence band edge. eqn (7) directly reveals that for p-type doping the magnitude of S decreases with increasing n, as shown in Fig. 5(a). In analogy, one can obtain a similar equation and explain the linear dependence displayed in the n-type case. It can be observed from Fig. 5(b) that the dependence of the Seebeck coefficient on carrier concentration deviates from the linear behavior and a local minimum appears. This could be attributed to the multi-band effect, which indicates that contributions of different bands to the Seebeck coefficient could have different signs and vary with temperature and doping concentration. We also evaluated the thermoelectric power factor $S^2\sigma/\tau$ of $\mathrm{CuInTe_2}$ in different crystallographic directions as a function of carrier concentration at three different temperatures of 300, 600 and 800 K. While $S^2\sigma/\tau$ of p-type $\mathrm{CuInTe_2}$ is nearly isotropic (Fig. 5(c)), there is considerable anisotropy in n-type one (Fig. 5(d)). Another key observation is that the optimized carrier concentration that maximizes $S^2\sigma/\tau$ depends on the temperature and as the temperature increases, higher carrier concentrations are required to maximize $S^2\sigma/\tau$.

Fig. 6 shows the Seebeck coefficient (a), electrical conductivity (b), thermal conductivity (c) and figure of merit (d) of p-type $\mathrm{CuInTe_2}$ as a function of temperature at different carrier concentrations. Fig. 6(a) shows that the Seebeck coefficient increases with increasing temperature, which is mainly because the term, $\exp[-(E_v - \varepsilon)/k_BT]$ with $\varepsilon < E_v$ in eqn (8) increases with increasing temperature and then leads to an increasing N_v. The calculated Seebeck coefficients are in reasonable agreement with the available experimental data with the carrier concentration value of $4.22 \times 10^{19}\ \mathrm{cm^{-3}}$ at 300 K.[12] There exists some discrepancy between theoretical and experimental data and it becomes remarkable at the higher temperature regime. This is most likely because the carrier concentrations of measured $\mathrm{CuInTe_2}$ samples vary with temperature due to the thermal excitation. The behavior that Seebeck coefficients first increase then reduce with increasing temperature has been reported in previous experimental studies.[32,33] At high temperatures electrons are thermally excited across the band gap and two different types of carriers participate in the transport, which is known as the bipolar effect. Then the total Seebeck coefficient is given by[34]

$$S = \frac{\sigma_e S_e + \sigma_h S_h}{\sigma_e + \sigma_h} \tag{9}$$

where S_e and S_h are the Seebeck coefficients of electrons and holes, respectively, and σ_e and σ_h are the electrical conductivities of electrons and holes, respectively. According to eqn (9), the Seebeck coefficient will be significantly suppressed because electrons and holes have opposite charges (S_e and S_h have opposite signs). In our calculations the carrier concentrations are instead kept fixed when the temperature increases by

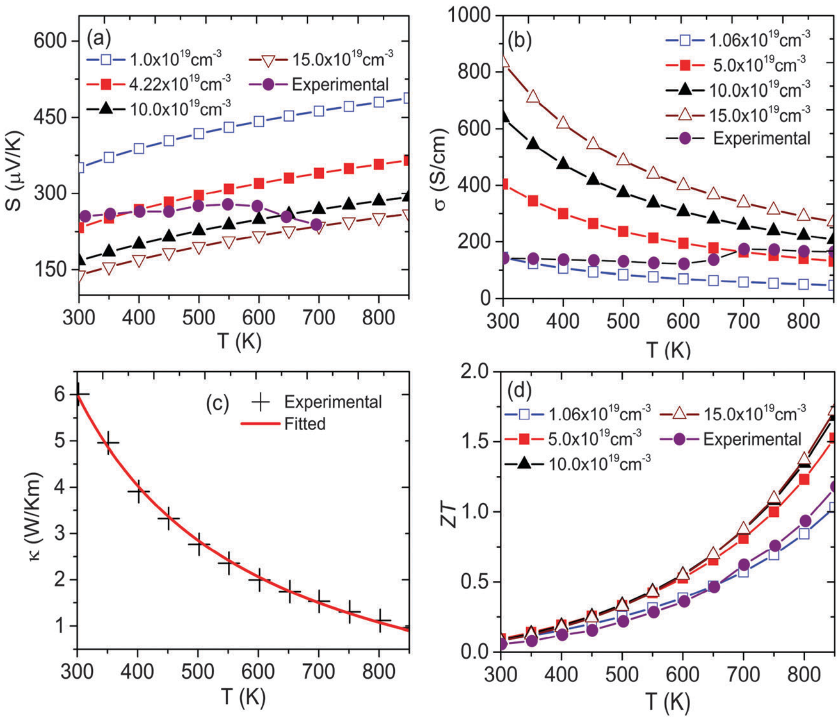

Fig. 6 Seebeck coefficient (a), electrical conductivity (b), phonon thermal conductivity (c) and figure of merit (d) of p-type $\mathrm{CuInTe_2}$ as a function of temperature at different carrier concentrations. The experimental data are plotted for comparison.

Published on 09 November 2015. Downloaded by Tsinghua University on 21/05/2018 02:33:05.

tuning the chemical potential in the Fermi–Dirac distribution function. We determined the charge carrier relaxation time empirically according to conductivity measurements in the previously published paper.[11] Generally the relaxation time τ depends on the temperature and carrier concentration,[11] and may be expressed as follows:[35]

$$\tau = \lambda n^{-1/3}T^{-1} \quad (10)$$

where n is the carrier concentration, T is the temperature and λ is a constant. Liu and co-workers reported an experimental electrical conductivity σ of 14431 S m^{-1} for CuInTe$_2$ with the carrier concentration of 1.06 × 10^{19} cm^{-3} at 300 K.[11] By comparing it with the calculated σ/τ, we obtain τ equal to 2.58 × 10^{-14} s at the same carrier concentration and temperature. Based on the obtained τ, one can determine λ and $\tau(n,T)$ as a function of carrier concentration and temperature. Fig. 6(b) shows the absolute value of electrical conductivity of CuInTe$_2$ obtained according to eqn (10). Since the scattering rate increases with temperature, the electrical conductivity decreases with increasing temperature. When the temperature is lower than 650 K, the calculated results agree well with the experimental data.[11] For the same reason discussed above (thermal excitation), the theoretical data deviate from the experimental observations in the higher temperature regime as shown in Fig. 6(b).

In the higher temperature limit, phonon scattering dominates the lattice thermal conductivity. The phonon thermal conductivity κ_L generally obeys T^{-1} Umklapp phonon scattering behavior.[35] Here, we fitted the thermal conductivity of CuInTe$_2$ by adopting the formula $\kappa = a + b/T$. The fitted thermal conductivity κ is plotted in Fig. 6(c), which matches well with the experimental data. The calculated figure of merit ZT of p-type CuInTe$_2$ as a function of temperature is shown in Fig. 6(d). Theoretically, the ZT displays an increasing trend with temperature. The calculated values are higher than the experimental data at same carrier concentrations (1.06 × 10^{19} cm^{-3}),[11] mainly originating from the fact that the calculated Seebeck coefficients are higher than the measured values (see Fig. 6(a)). Overall, CuInTe$_2$-based materials under the optimal level of doping are very promising for thermoelectric applications in the medium temperature range.

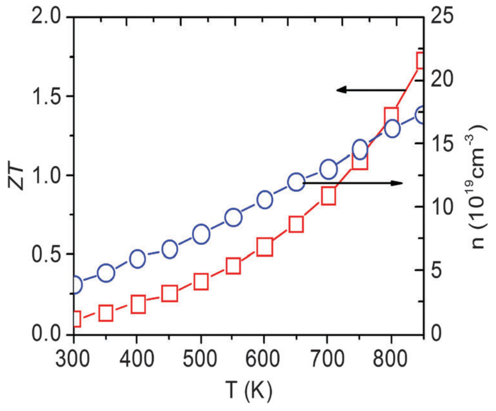

Fig. 7 Optimized figure of merit of p-type CuInTe$_2$ and the corresponding carrier concentrations as a function of temperature.

The upper bound value for ZT and the corresponding carrier concentration as a function of temperature are shown in Fig. 7. Both the optimized ZT and the corresponding carrier concentration increase with increasing temperature. p-type CuInTe$_2$ can achieve the highest optimized ZT value of 1.72 at 850 K, which is fairly high and implies an energy-conversion performance comparable to that of commercially available thermoelectric materials. The corresponding optimized carrier concentration increases with temperature and changes in the range from 5 × 10^{19} to 20 × 10^{19} cm^{-3}.

Conclusions

In conclusion, we have performed density functional calculations on the CuInTe$_2$ system and analyzed its band structures, and phonon and thermoelectric transport properties. From the analysis of DOS and partial charge density, it is found that there exist three-dimensional [–Cu–Te–Cu–] and [–In–Te–In–] conducting networks to act as the channels for hole transport and electron transport, respectively. Moreover, In-site and Cu-site doping are suitable for tuning carrier concentrations without unduly damage to the hole and electron transport networks, respectively. Lattice-dynamics calculations indicate that introducing structural defects at Cu, In or Te sites may prove effective in reducing the lattice thermal conductivity, and the calculated phonon frequencies also agree with the experimental data. p-type CuInTe$_2$ exhibits better thermoelectric properties as compared to the n-type one, which mainly originates from the steeper DOS resulting from nearly degenerate valence bands near the edge of the valence band. The dependence of thermoelectric transport properties on the doping level and temperature was investigated in detail, which provides a guidance for future experiments to optimize the ZT values of CuInTe$_2$. We predicted that p-type CuInTe$_2$ could exhibit high thermoelectric performance by optimizing hole-doped carrier concentrations, and the corresponding optimized carrier concentration is in the range of 5 × 10^{19} cm^{-3} to 20 × 10^{19} cm^{-3}.

Acknowledgements

This work was supported by China Postdoctoral Science Foundation (Grant No. 2012M520236) and National Natural Science Foundation of China (Grant No. 21273124 and 21290190). Computational resources were provided by Tsinghua National Laboratory for Information Science and Technology of China.

References

1 K. Biswas, J. He, I. D. Blum, C.-I. Wu, T. P. Hogan, D. N. Seidman, V. P. Dravid and M. G. Kanatzidis, *Nature*, 2012, **489**, 414–418.

Published on 09 November 2015. Downloaded by Tsinghua University on 21/05/2018 02:33:05.

2 M. S. Dresselhaus, G. Chen, M. Y. Tang, R. Yang, H. Lee, D. Wang, Z. Ren, J. P. Fleurial and P. Gogna, *Adv. Mater.*, 2007, **19**, 1043–1053.

3 G. J. Snyder and E. S. Toberer, *Nat. Mater.*, 2008, **7**, 105–114.

4 J. P. Heremans, V. Jovovic, E. S. Toberer, A. Saramat, K. Kurosaki, A. Charoenphakdee, S. Yamanaka and G. J. Snyder, *Science*, 2008, **321**, 554–557.

5 J. P. Heremans, M. S. Dresselhaus, L. E. Bell and D. T. Morelli, *Nat. Nanotechnol.*, 2013, **8**, 471–473.

6 G. Zhou, L. Li and G. Li, *Appl. Phys. Lett.*, 2010, **97**, 3112.

7 X. Shi, J. Yang, J. R. Salvador, M. Chi, J. Y. Cho, H. Wang, S. Bai, J. Yang, W. Zhang and L. Chen, *J. Am. Chem. Soc.*, 2011, **133**, 7837–7846.

8 D. Wu, L.-D. Zhao, X. Tong, W. Li, L. Wu, Q. Tan, Y. Pei, L. Huang, J.-F. Li and Y. Zhu, *Energy Environ. Sci.*, 2015, **8**, 2056–2068.

9 A. Majumdar, *Science*, 2004, **303**, 777–778.

10 Y. He, T. Day, T. Zhang, H. Liu, X. Shi, L. Chen and G. J. Snyder, *Adv. Mater.*, 2014, **26**, 3974–3978.

11 R. Liu, L. Xi, H. Liu, X. Shi, W. Zhang and L. Chen, *Chem. Commun.*, 2012, **48**, 3818–3820.

12 H. Chen, C. Yang, H. Liu, G. Zhang, D. Wan and F. Huang, *CrystEngComm*, 2013, **15**, 6648–6651.

13 J. Yang, S. Chen, Z. Du, X. Liu and J. Cui, *Dalton Trans.*, 2014, **43**, 15228–15236.

14 J. Yan, P. Gorai, B. Ortiz, S. Miller, S. A. Barnett, T. Mason, V. Stevanović and E. S. Toberer, *Energy Environ. Sci.*, 2015, **8**, 983–994.

15 G. Kresse and J. Hafner, *Phys. Rev. B: Condens. Matter Mater. Phys.*, 1993, **47**, 558.

16 G. Kresse and J. Furthmüller, *Comput. Mater. Sci.*, 1996, **6**, 15–50.

17 G. Kresse and J. Furthmüller, *Phys. Rev. B: Condens. Matter Mater. Phys.*, 1996, **54**, 11169.

18 J. P. Perdew, J. Chevary, S. Vosko, K. A. Jackson, M. R. Pederson, D. Singh and C. Fiolhais, *Phys. Rev. B: Condens. Matter Mater. Phys.*, 1992, **46**, 6671.

19 Y. Zhang, X. Yuan, X. Sun, B.-C. Shih, P. Zhang and W. Zhang, *Phys. Rev. B: Condens. Matter Mater. Phys.*, 2011, **84**, 075127.

20 A. Togo, F. Oba and I. Tanaka, *Phys. Rev. B: Condens. Matter Mater. Phys.*, 2008, **78**, 134106.

21 G. K. Madsen and D. J. Singh, *Comput. Phys. Commun.*, 2006, **175**, 67–71.

22 N. W. Ashcroft and N. D. Mermin, *Solid State Physics*, Holt, Rinehart and Winston, New York, 1976.

23 D. Parker and D. J. Singh, *Phys. Rev. B: Condens. Matter Mater. Phys.*, 2012, **85**, 125209.

24 A. F. May, D. J. Singh and G. J. Snyder, *Phys. Rev. B: Condens. Matter Mater. Phys.*, 2009, **79**, 153101.

25 L. Xi, Y. Zhang, X. Shi, J. Yang, X. Shi, L. Chen, W. Zhang, J. Yang and D. J. Singh, *Phys. Rev. B: Condens. Matter Mater. Phys.*, 2012, **86**, 155201.

26 G. Zhou and D. Wang, *Sci. Rep.*, 2015, **5**, 8099.

27 G. Mahan and J. Sofo, *Proc. Natl. Acad. Sci. U. S. A.*, 1996, **93**, 7436–7439.

28 C. Rincón, S. Wasim, G. Marın, E. Hernández, J. Delgado and J. Galibert, *J. Appl. Phys.*, 2000, **88**, 3439–3444.

29 K. Biswas and C. W. Myles, *Phys. Rev. B: Condens. Matter Mater. Phys.*, 2007, **75**, 245205.

30 G. Lan, B. Ouyang and J. Song, *Acta Mater.*, 2015, **91**, 304–317.

31 G. Zhou, L. Li and G. Li, *J. Appl. Phys.*, 2011, **109**, 114311.

32 D. Kraemer, J. Sui, K. McEnaney, H. Zhao, Q. Jie, Z. Ren and G. Chen, *Energy Environ. Sci.*, 2015, **8**, 1299–1308.

33 L.-D. Zhao, S.-H. Lo, Y. Zhang, H. Sun, G. Tan, C. Uher, C. Wolverton, V. P. Dravid and M. G. Kanatzidis, *Nature*, 2014, **508**, 373–377.

34 D. B. Luo, Y. X. Wang, Y. L. Yan, G. Yang and J. M. Yang, *J. Mater. Chem. A*, 2014, **2**, 15159–15167.

35 K. P. Ong, D. J. Singh and P. Wu, *Phys. Rev. B: Condens. Matter Mater. Phys.*, 2011, **83**, 115110.